Fatigue failure prediction in lattice structures through numerical method based on de-homogenization process

Available online at www.sciencedirect.com

ScienceDirect

Procedia Structural Integrity 41 (2022) 535–543

Structural Integrity Procedia

www.elsevier.com/locate/procedia

2nd Mediterranean Conference on Fracture and Structural Integrity

Fatigue failure prediction in lattice structures through numerical method based on de-homogenization process

Giorgio De Pasquale*, Antonio Coluccia

Department of Mechanical and Aerospace Engineering, Politecnico di Torino, Corso Duca degli Abruzzi 24, 10129, Torino (Italy)

Abstract

Metal lattice structures from additive manufacturing (AM) processes are promising solutions for the design of lightweight components and therefore several strategies for their static modeling are available. However, the high concentration of notches, combined to the surface roughness typical of AM as-built conditions, make lattice structures very vulnerable to fatigue failures. Furthermore, the evaluation of stress and strain in cellular materials is very challenging due to the geometrical complexity and the associated computational heaviness of numerical models. In this paper, the authors present a numerical method based on the homogenization and de-homogenization processes to determine the expected fatigue lifetime of the lattice component. The method requires limited computational effort by limiting the estimation to the most loaded cell, which is considered as representative volume element (RVE) to establish the multi-axial fatigue loads.

Keywords: Lattice structures; lightweight design; additive manufacturing; fatigue; FEM.

1. Introduction

Cellular solids have been widely exploited in the last decades due to their excellent peculiar mechanical properties and functionality. Among them, lattice structures recently emerged especially in relation to the

* Corresponding author. Tel.: 011.090.6452.
E-mail address: giorgio.depasquale@polito.it

10.1016/j.prostr.2022.05.061

consolidation and technological improvement of additive manufacturing (AM) processes. According to the definition found in the investigation by Fleck et al. (2010), lattice materials are "cellular, reticulated, truss or lattice structure made up of a large number of uniform lattice elements and generated by tessellating a unit cell". They consist of a repetition of a defined representative volume element (RVE) containing a specified unit cell. The AM technology can support high levels of design freedom, and then the designer can conceive many topologies of cells to build the lightweight component. Literature is rich with examples of experimental investigations and mechanical characterization of lattice structures as it can be seen in contributions from De Pasquale et al.(2019), Lei et al. (2019) and De Pasquale and Luceri (2019), often necessary to develop designs which can found application in many engineering sectors. Biomedical engineering is of course one of the most important: due to their manufacturability, integration with bones and mechanical properties, lattices are largely used for prosthetic implants, as defined from Wang er al. (2018). Mechanical application can also be found in the automotive sector, e.g. the design proposed from Yin et al. (2018), as the core of sandwich panels for car hoods. Aerospace engineering also benefit from the application of such structures: De Pasquale and Tagliaferri (2021) furnish a design presenting lattice structures as impact absorber, and at the same time heat exchanger.

Though AM is nowadays able to create high quality components, as described from De Pasquale (2021), problems regarding microstructural features and defects due to the AM processes are present. Due to their shape, lattice cells are defined at the mesoscale, typically in the order of millimeters, and generally have complex topology. Then, researchers are focused on improving the mechanical properties of these structures through the enhancement of their topological characteristics. Among all, truss lattices present severe problems because of their high concentration of sharp corners and notches, together with the surface roughness due to the AM as-built properties. These are issues to deal with when it comes to reliability performances. In particular, fatigue failure analysis is extremely important, since the lattice characteristics listed before largely tend to favor stress concentrations and cracks initiation and propagation, as Gu et al. (2019) show.

Finite element method (FEM) is often used for fatigue failure analyses, but when it comes to large lattice structures made of thousands unit cells, the 3D simulation become computationally heavy and unpractical. A lighter method for fatigue lifetime prediction based on FEM is presented in this paper. By applying a linear homogenization process, used for composite materials and cellular solids as well, lattices are modeled as orthotropic medium material. Therefore, the complex lattice structure is represented by means of simpler elements with customized stiffness matrix, with far less elements than the full 3D model would require. Homogenization is extremely useful when it comes to static and dynamic analyses as well. Once the structure is homogenized, static simulations are performed. From the static results, the most critical cell is identified, and reverse homogenization is applied on it. The strain condition of one single cell, extracted from the results given by the homogenized medium, is applied to the real 3D model of the cell, by implementing a de-homogenization process. The real stress distribution is then calculated, and the three-axial most loaded point of the structure is determined quantitatively. In correspondence to this point, one multiaxial fatigue method is applied, according to the stress state present there. In this paper, the Crossland and Sines methods are suggested for this purpose. The calculation algorithm is finally implemented in the Ansys software environment to provide practical simulation tool for the designer.

2. Method

The method is applicable to general shaped lattice structure composed by given RVE. In this section, the analytic formulation of the method for fatigue lifetime estimation is described.

2.1. Homogenization

The homogenization process, described in detail by Barbero (2013) as belonging to the field of computational micromechanics, can be applied to composites, lattice structure and any other material based on space-periodic repetition of one RVE including two or more structural domains or phases. The aim of homogenization is to extract the stiffness matrix linked with the RVE of the material considered for the process; from the stiffness matrix, equivalent material properties can be extracted and employed for a numerical model.

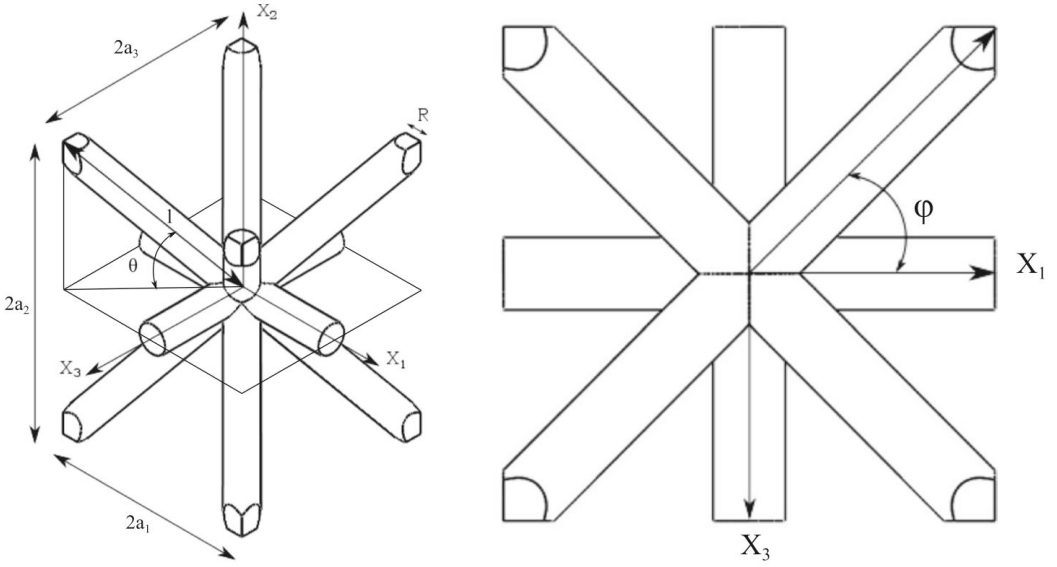

Fig. 1. Representation of the RVE, with relevant parameters for the homogenization process (a1, a2, a3).

By considering the generic lattice cell (e.g., that one represented in Fig. 1 with its own dimensional parameters, material properties and topology), six static simulations can be performed with specific boundary conditions to calculate the terms of the stiffness matrix [C] correlating the average stress $\{\bar{\sigma}\}$ and average strain $\{\bar{\varepsilon}\}$ tensors (1).

$$\begin{Bmatrix} \overline{\sigma_1} \\ \overline{\sigma_2} \\ \overline{\sigma_3} \\ \overline{\sigma_4} \\ \overline{\sigma_5} \\ \overline{\sigma_6} \end{Bmatrix} = \begin{bmatrix} C_{11} & \cdots & C_{16} \\ C_{21} & \cdots & C_{26} \\ \vdots & \ddots & \vdots \\ C_{61} & \dots & C_{66} \end{bmatrix} \begin{Bmatrix} \overline{\varepsilon_1} \\ \overline{\varepsilon_2} \\ \overline{\varepsilon_3} \\ \overline{\gamma_4} \\ \overline{\gamma_5} \\ \overline{\gamma_6} \end{Bmatrix} \tag{1}$$

The shear strains are defined as:

$$\overline{\gamma_\iota} = \overline{\varepsilon_{\iota j}} + \overline{\varepsilon_{\iota J}} \quad with\ i,j = 1,2,3 \tag{2}$$

On the RVE, the hypothesis of constant strain energy is applied to define the homogenized stiffness matrix, because, when deforming, both original cell and homogenized cell will be defined by the same amount of strain energy. Also, each one of the six applied strain components ε_β^0 is averaged on the RVE volume (average strain $\overline{\varepsilon_\beta}$), according to Eq. (3). The six different linear elastic Eqs. (1) must be solved six times, each one of them with only one non-zero strain component (4). More in detail, the boundary conditions of each static analysis necessary for the definition of the strain condition aforementioned are described in Tab. 1 (each column reports one boundary conditions set) and Eqs. (5)-(7).

$$\overline{\varepsilon_\iota} = \frac{1}{V}\int_V \varepsilon_i dV = \varepsilon_i^0 \tag{3}$$

$$C_{\alpha\beta} = \overline{\sigma_\alpha} = \int_V \sigma_\alpha(x_1, x_2, x_3) dV \quad where\ \varepsilon_\beta^0 = 1 \quad for\ \alpha, \beta = 1, \dots, 6 \tag{4}$$

Table 1. Summary of boundary conditions applied on the RVE for the calculation of the stiffness matrix components: *Ui* terms represents the displacement degrees of freedom (DOF) of the nodes of the RVE in the system (x_1, x_2, x_3), "0" = constrained DOF, "/" = free DOF.

RVE face	*1st analysis*			*2nd analysis*			*3rd analysis*			*4th analysis*			*5th analysis*			*6th analysis*		
	$\bar{\varepsilon}_1 = 1$			$\bar{\varepsilon}_2 = 1$			$\bar{\varepsilon}_3 = 1$			$\bar{\gamma}_4 = 1$			$\bar{\gamma}_5 = 1$			$\bar{\gamma}_6 = 1$		
	U_1	U_2	U_3	U_1	U_2	U_3	U_1	U_2	U_3	U_1	U_2	U_3	U_1	U_2	U_3	U_1	U_2	U_3
$\boldsymbol{x_1 = -a_1}$	$-a_1$	/	/	0	/	/	0	/	/	0	/	/	/	0	$-a_1$	/	$-a_1$	0
$\boldsymbol{x_1 = a_1}$	a_1	/	/	0	/	/	0	/	/	0	/	/	/	0	a_1	/	a_1	0
$\boldsymbol{x_2 = -a_2}$	/	0	/	/	$-a_2$	/	/	0	/	0	/	$-a_2$	/	0	/	$-a_2$	/	0
$\boldsymbol{x_2 = a_2}$	/	0	/	/	a_2	/	/	0	/	0	/	a_2	/	0	/	a_2	/	0
$\boldsymbol{x_3 = -a_3}$	/	/	0	/	/	0	/	/	$-a_3$	0	$-a_3$	/	$-a_3$	0	/	/	/	0
$\boldsymbol{x_3 = a_3}$	/	/	0	/	/	0	/	/	a_3	0	a_3	/	a_3	0	/	/	/	0

For each static analysis, one strain component is set to the unity, with reference to the imposed boundary displacement conditions. The strain components of the RVE are described as follows:

$$\begin{cases} u_1(a_1,x_2,x_3) - u_1(-a_1,x_2,x_3) = 2a_1\varepsilon_{11}^0 \\ u_2(a_1,x_2,x_3) - u_2(-a_1,x_2,x_3) = 2a_1\varepsilon_{21}^0 \\ u_3(a_1,x_2,x_3) - u_3(-a_1,x_2,x_3) = 2a_1\varepsilon_{31}^0 \end{cases}$$
$$\begin{cases} u_1(x_1,a_2,x_3) - u_1(x_1,-a_2,x_3) = 2a_2\varepsilon_{12}^0 \\ u_2(x_1,a_2,x_3) - u_2(x_1,-a_2,x_3) = 2a_2\varepsilon_{22}^0 \\ u_3(x_1,a_2,x_3) - u_3(x_1,-a_2,x_3) = 2a_2\varepsilon_{32}^0 \end{cases} \quad (5)$$
$$\begin{cases} u_1(x_1,x_2,a_3) - u_1(x_1,x_2,-a_3) = 2a_3\varepsilon_{13}^0 \\ u_2(x,x_2,a_3) - u_2(x_1,x_2,-a_3) = 2a_3\varepsilon_{23}^0 \\ u_3(x_1,x_2,a_3) - u_3(x_1,x_2,-a_3) = 2a_3\varepsilon_{33}^0 \end{cases}$$

Every edge belongs at the same time to two faces, and since only one constraint equation can be established for a geometrical feature, edges need their own set of conditions, defined by Eqs. (6):

$$\begin{cases} u_i(a_1,a_2,x_3) - u_i(-a_1,-a_2,x_3) = 2a_1\varepsilon_{i1}^0 + 2a_2\varepsilon_{i2}^0 \\ u_i(a_1,-a_2,x_3) - u_i(-a_1,a_2,x_3) = 2a_1\varepsilon_{i1}^0 - 2a_2\varepsilon_{i2}^0 \end{cases} \quad with\ i = 1,2,3$$
$$\begin{cases} u_i(a_1,x_2,a_3) - u_i(-a_1,x_2,-a_3) = 2a_1\varepsilon_{i1}^0 + 2a_3\varepsilon_{i3}^0 \\ u_i(a_1,x_2,-a_3) - u_i(-a_1,x_2,a_3) = 2a_1\varepsilon_{i1}^0 - 2a_3\varepsilon_{i3}^0 \end{cases} \quad with\ i = 1,2,3 \quad (6)$$
$$\begin{cases} u_i(x_1,a_2,a_3) - u_i(x_1,-a_2,-a_3) = 2a_2\varepsilon_{i2}^0 + 2a_3\varepsilon_{i3}^0 \\ u_i(x_1,a_2,-a_3) - u_i(x_1,-a_2,a_3) = 22\varepsilon_{i2}^0 - 2a_3\varepsilon_{i3}^0 \end{cases} \quad with\ i = 1,2,3$$

Similar consideration is valid for the corners, which need their own conditions:

$$\begin{cases} u_i(a_1,a_2,a_3) - u_i(-a_1,-a_2,-a_3) = 2a_1\varepsilon_{i1}^0 + 2a_2\varepsilon_{i2}^0 + 2a_3\varepsilon_{i3}^0 \\ u_i(a_1,a_2,-a_3) - u_i(-a_1,-a_2,a_3) = 2a_1\varepsilon_{i1}^0 + 2a_2\varepsilon_{i2}^0 - 2a_3\varepsilon_{i3}^0 \\ u_i(-a_1,a_2,a_3) - u_i(a_1,-a_2,-a_3) = -2a_1\varepsilon_{i1}^0 + 2a_2\varepsilon_{i2}^0 + 2a_3\varepsilon_{i3}^0 \\ u_i(a_1,-a_2,a_3) - u_i(-a_1,a_2,-a_3) = 2a_1\varepsilon_{i1}^0 - 2a_2\varepsilon_{i2}^0 + 2a_3\varepsilon_{i3}^0 \end{cases} \quad with\ i = 1,2,3 \quad (7)$$

Equations (4), (5) and (6) gives all the constraints necessary to the static analyses representing the homogenization process. From the results, the components of the average stress field $\overline{\sigma_\alpha}$ are obtained and by means

of Eq. (4), the terms of the stiffness matrix are calculated. The compliance matrix is calculated from Eq. (8) and the equivalent material properties are obtained by the relations of Eqs. (9), (10) and (11).

$$[S] = [C]^{-1} \quad (8) \tag{8}$$

$$E_1 = \frac{1}{S_{11}} \quad E_2 = \frac{1}{S_{22}} \quad E_3 = \frac{1}{S_{33}} \quad (9) \tag{9}$$

$$G_{23} = \frac{1}{S_{44}} \quad G_{13} = \frac{1}{S_{55}} \quad G_{12} = \frac{1}{S_{66}} \quad (10) \tag{10}$$

$$\nu_{12} = -S_{12} \cdot E_1 \quad \nu_{23} = -S_{23} \cdot E_2 \quad \nu_{13} = -S_{13} \cdot E_1 \quad (11) \tag{11}$$

2.2. Identification of the most loaded cell and de-homogenization process

The lattice structure is now effectively modeled through the equivalent material properties given by Eqs. (9), (10) and (11). The analysis of each RVE is significantly lighter and requires just one finite element to be discretized. The full 3D model of the structure with homogeneous medium material replacing the lattice is defined. The nominal fatigue load is applied to this model by separating the mean and alternate loads, considered as two static load components. Each load component will provide the corresponding strain distribution in the homogenized medium, which is then converted into local mean and alternate stress.

Thus, the elastic strain tensor is computed on the homogeneous media as

$$[\varepsilon] = \begin{bmatrix} \varepsilon_{xx} & \varepsilon_{xy} & \varepsilon_{xz} \\ \varepsilon_{yx} & \varepsilon_{yy} & \varepsilon_{yz} \\ \varepsilon_{zx} & \varepsilon_{zy} & \varepsilon_{zz} \end{bmatrix} \tag{12}$$

The norm of the strain tensor (13) is therefore evaluated for every element of the homogeneous media:

$$\|\varepsilon\| = \sqrt{\sum_i \sum_j \varepsilon_{ij} \cdot \varepsilon_{ij}} \tag{13}$$

and the most loaded (or critical) cell of the homogeneous media is identified as the one with the higher $\|\varepsilon\|$. This step is significant to limit the extension of the further analysis just to the cell that is the first candidate to exhibit fatigue failure. The other cells will have lower stress levels and then longer expected fatigue lifetime. Then, the lifetime of the entire structure is imposed by the lifetime of the most critical cell only.

The next step of the method is the de-homogenization of the critical cell. The strain field produced on the critical cell by the application of the external nominal loads (mead and average separately) is stored. A 3D full static model of the RVE with its real shape (e.g., that one in Fig. 1) is built, and the mentioned strain field of Eq. (12) is applied at the corresponding boundaries. The model returns the 3-dimensional stress distribution expected in the critical cell of the structure. The most loaded point of the volume is identified and the local multi-axial stress components stored.

2.3. Application of failure criteria

The most loaded point of the structure is then defined, and two sets of multi-axial stress are calculated, provided by the nominal mean and alternate external load components respectively. At this stage, one of the multi-axial fatigue methods can be applied to estimate the fatigue life of the structure, through the analysis of its critical point. In the following, two methods are proposed: Crossland and Sines.

Crossland fatigue method

The Crossland (1956) multi-axial fatigue method is based on the equivalent stress (14), defined from the principal stresses along the three directions. The Crossland equivalent stress must be lower than the fatigue torsional limit (τ_f) to have endless life.

$$\tau_{CROSS,eq} = \sqrt{J_{2,a}} + \left(\frac{3\tau_f}{\sigma_f} - \sqrt{3}\right)\sigma_{H,max} \leq \tau_f \tag{14}$$

The Crossland stress is calculated from shear and bending (σ_f) fatigue limits, the second invariant of the deviatoric stress tensor ($J_{2,a}$) expressed by Eq. (15) and the maximum hydrostatic stress ($\sigma_{H,max}$) from Eq. (16).

$$\sqrt{J_{2,a}} = \frac{\sigma_{eq}}{\sqrt{3}} \tag{15}$$

$$\sigma_{H,max} = \frac{S_1+S_2+S_3}{3} \tag{16}$$

In Eqs. (15) and (16), σ_{eq} is the equivalent stress, while S_1, S_2 and S_3 are the principal stresses along the three principal directions. The Crossland method is very easy to be computed, but reliable parameters of torsional fatigue limit are not easy to find for many materials, and sometimes the physical links to the effective structural loads are not so evident, as stated from Navarro et al. (2007), for instance the missing separation of the effects of mean and alternate stress.

Sines fatigue method

The Sines (1955) fatigue method in multi-axial loading conditions defines two equivalent stress values, mean and alternate respectively. The method is based on the second alternating stress invariant and the first medium stress invariant, as expressed by Eq. (17):

$$\sqrt{J_{2,a}} \leq B - \beta J_{1,m} \tag{17}$$

where B and β are two constants related to the fatigue limit and static strength respectively. This expression can be translated in terms of principal stresses as

$$\frac{1}{\sqrt{2}}\sqrt{\left(\sigma_{a,1}-\sigma_{a,2}\right)^2 + \left(\sigma_{a,1}-\sigma_{a,3}\right)^2 + \left(\sigma_{a,2}-\sigma_{a,3}\right)^2} + \frac{\sigma_{D-1}}{R_m}(\sigma_{m,1}+\sigma_{m,2}+\sigma_{m,3}) \leq \sigma_{D-1} \tag{18}$$

Here, $\sigma_{a,i}$ and $\sigma_{m,i}$ are the alternate and mean principal stresses respectively, σ_{D-1} is the fatigue limit and R_m is the static strength of the material. This method is based on the effects of shear stress on the slippage of single crystals in the material. From Sines theory, equivalent alternate and mean stress can be calculated from Eq. (19) and Eq. (20) respectively, and used to define a working point in the Haigh diagram.

$$\sigma_{a,eq} = \frac{1}{\sqrt{2}}\sqrt{\left(\sigma_{a,1}-\sigma_{a,2}\right)^2 + \left(\sigma_{a,1}-\sigma_{a,3}\right)^2 + \left(\sigma_{a,2}-\sigma_{a,3}\right)^2} \tag{19}$$

$$\sigma_{m,eq} = (\sigma_{m,1}+\sigma_{m,2}+\sigma_{m,3}) \tag{20}$$

3. FEM model

The method described in section 2 is used to compute the fatigue stress on two lattice specimens. The method has been implemented into a macro for the ANSYS environment, to provide easy and fast tool for simulation of fatigue life prediction. The two samples considered have been designed for further experimental validation, and they are composed by two bulk ends and lattice center. In one case the lattice is uniform, in the other case the lattice is graded by varying the cells size. The total dimension of the sample is 90x30x4 mm^3, the lattice section dimension is 36.7x30x4 mm^3 where the total number of cells is 14x15x2. The cell shape is the same reported in Fig. 1. In the sample with uniform lattice, dimensional parameters are $l = 2mm$, $\theta = \varphi = 45°$ therefore $a_1 = a_3 = l/2 = 1mm$ and $a_2 = l \cdot \sin\theta = 1.414$ mm, while standard strut diameter, used for uniform lattice, is $0.5\,mm$. Graded lattice

presents instead an increasing diameter going from the middle to the bottom section of the sample, while standard diameter is used from the middle to the top section. In order to allow continuity in the intersection nodes of the lattice, a single cell presents two diameters, as it can be seen in figure 2c. Diameters for the graded section are in a range from 0.5 (nominal) to 1.1 and those are defined in Tab. 2 as well.

In Fig. 2a, the two structures are represented. The material considered is the simulations is Inconel-625 alloy, whose properties are listed in Tab. 2.

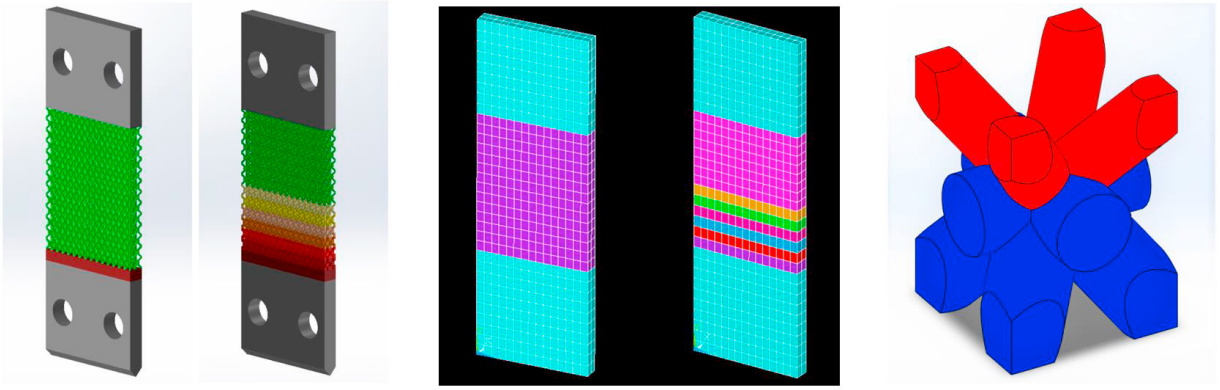

Fig. 2. Samples geometry with uniform and graded lattice *(a)*. Homogenized models where colors different from light blue (that is bulk material) represent homogenized materials; for the graded sample (right), colors going from purple (bottom) to the pink (top) represents cells where diameter is decreasing from 1.1 mm to 0.5 mm *(b)*. Example of a single cell for the graded sample, where the diameter switch happens in the middle of the cell in order to guarantee continuity at the nodes *(c)*.

In the first step of the method, the lattice homogenization is provided to every RVE of the two samples. For the uniform lattice, the same homogenized media is defined everywhere; for the graded lattice, the RVE homogeneous media is variable with the original cell properties, as it can be seen in Fig. 2b. For the latter case, the calculated structural properties are reported in Tab. 2

Table 2. Material properties of Inconel-625, and material properties of the homogenized lattice cells, together with relative diameters.

Properties	*Inconel-625*	*Properties*	*Cell 1*	*Cell 2*	*Cell 3*	*Cell 4*	*Cell 5*	*Cell 6*	*Cell 7*
		Upper/lower diameter [mm]	*0.5/0.5 (uniform)*	*0.5/0.6*	*0.6/0.7*	*0.7/0.8*	*0.8/0.9*	*0.9/1*	*1/1.1*
E [GPa]	205	E_1***[GPa]***	11.092	16.631	26.226	39.968	58.643	82.057	108.527
		E_2***[GPa]***	11.946	16.257	26.344	40.575	59.344	82.304	108.025
		E_3***[GPa]***	11.092	16.627	26.209	39.943	58.607	82.163	108.514
ν	0.308	G_{12}***[GPa]***	8.343	10.178	14.935	20.874	27.912	35.962	44.800
		G_{13}***[GPa]***	5.283	7.165	11.344	17.102	24.639	33.853	43.913
		G_{23}***[GPa]***	8.343	10.178	14.947	20.862	27.929	35.979	44.603
G[GPa]	78.364	ν_{12}	0.404	0.385	0.352	0.324	0.300	0.284	0.277
		ν_{13}	0.103	0.120	0.144	0.167	0.192	0.219	0.248
		ν_{23}	0.435	0.376	0.354	0.329	0.304	0.285	0.276

In the next step, the static analyses under nominal mean and average loads separately are conducted on the homogenized structures. In the present case, the samples are loaded with bending force at one end and constrained at the opposite end, in the cantilever configuration. The alternate load (100 N) provides the simulation results reported in Fig. 3. Each element corresponds to one cell here, then the strain tensor norm of Eq. (13) can be easily represented for the two samples. The highest value of this parameter is associated to the critical cells.

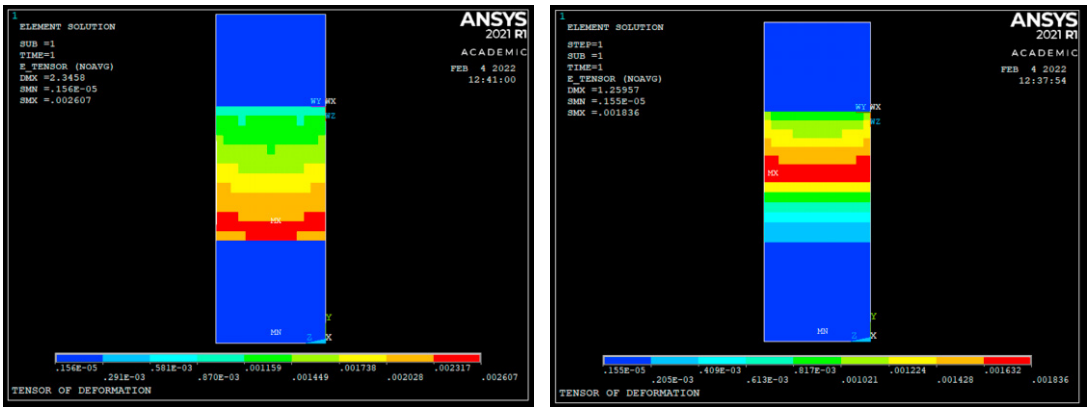

Fig. 3. Strain tensor norm contour for the two samples after static analysis under the alternated load (100 N) component.

The same analysis is provided for the strain distribution under the mean load component. In case of zero mean load, the previous one is the only strain contribution imposed to the homogenized lattice.

The critical cells are situated at one side of the uniform lattice (i.e. the side of the sample near the clamped end of the cantilever), and approximately in the middle of the graded lattice (where the balance between external bending moment and lattice density gives the critical situation).

The last step is de-homogenization and failure analysis, which is performed by using the Crossland method. The strain field is extracted from the most critical cell and applied to the real 3D geometry of the RVE. The Crossland equivalent stress of Eq. (14) is calculated and reported in Fig. 4. In this case, the stress results need to be compared to the torsional fatigue limit of the material.

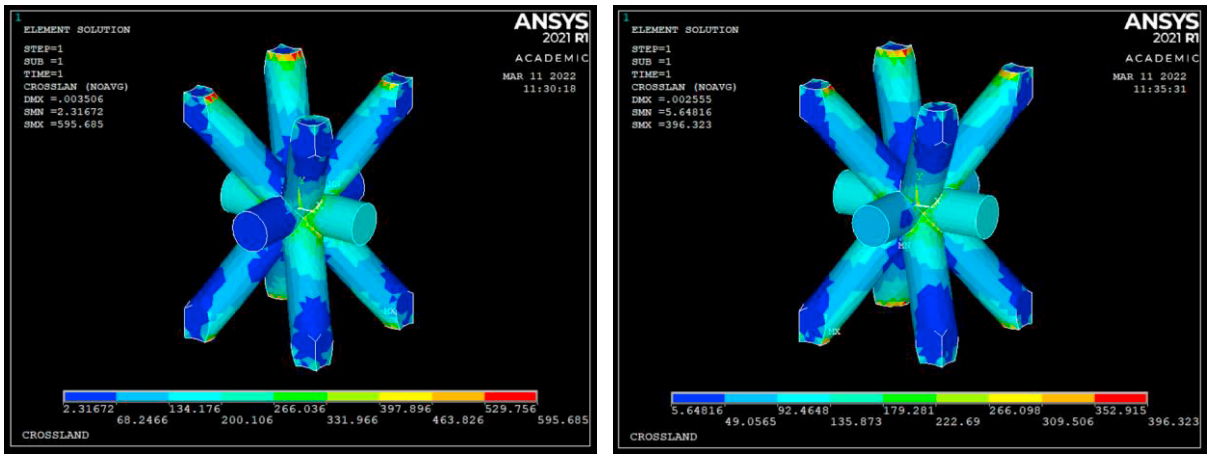

Fig. 4. Crossland equivalent stress contour of the most critical cell for the homogeneous (left) and graded (right) samples.

4. Conclusions

A method for fatigue lifetime estimation is introduced, which has the advantage of simplicity, even for topologically complex lattice structures. The linear static analysis is used to operate the lattice homogenization, to identify the most loaded (or critical) cell through the maximum value of strain tensor norm. The de-homogenization is then used to calculate the effective multi-axial stress components in the real cell and to apply the multi-axial fatigue methods. The method has been implemented into a macro for the Ansys environment and validated on two ideal structures with uniform and graded lattice shape.

References

N. A. Fleck, V. S. Deshpande, and M. F. Ashby, 2010. Micro-architectured materials: Past, present and future, Proc. R. Soc. A Math. Phys. Eng. Sci., vol. 466, no. 2121, pp. 2495–2516.

G. De Pasquale, F. Luceri, and M. Riccio, 2019. Experimental Characterization of SLM and EBM Cubic Lattice Structures for Lightweight Applications, Exp. Mech., vol. 59, no. 4, pp. 469–482.

H. Lei et al., 2019. Evaluation of compressive properties of SLM-fabricated multi-layer lattice structures by experimental test and μ-CT-based finite element analysis, Mater. Des., vol. 169, p. 107685.

G. De Pasquale and F. Luceri, 2019. Experimental validation of Ti6Al4V bio-inspired cellular structures from additive manufacturing processes, Mater. Today Proc., vol. 7, pp. 566–571.

Y. Wang, S. Arabnejad, M. Tanzer, and D. Pasini, 2018. Hip implant design with three-dimensional porous architecture of optimized graded density, J. Mech. Des. Trans. ASME, vol. 140, no. 11, pp. 1–13.

S. Yin, H. Chen, Y. Wu, Y. Li, and J. Xu, 2018. Introducing composite lattice core sandwich structure as an alternative proposal for engine hood, Compos. Struct., vol. 201, no. May, pp. 131–140.

G. De Pasquale and A. Tagliaferri, 2021. Modeling and characterization of mechanical and energetic elastoplastic behavior of lattice structures for aircrafts anti-icing systems, Proc. Inst. Mech. Eng. Part C J. Mech. Eng. Sci., vol. 235, no. 10, pp. 1828–1839.

G. De Pasquale, 2021. Additive Manufacturing of Micro-Electro-Mechanical Systems (MEMS), Micromachines, vol. 12, no. 1374.

H. Gu, S. Li, M. Pavier, M. M. Attallah, C. Paraskevoulakos, and A. Shterenlikht, 2019. Fracture of three-dimensional lattices manufactured by selective laser melting, Int. J. Solids Struct., vol. 180–181, pp. 147–159.

G. D. E. Pasquale, E. Bertuccio, A. Catapano, and M. Montemurro, 2019. Modeling of cellular structures under static and fatigue loads, II Int. Conf. Simul. Addit. Manuf. - Sim-AM 2019.

E. J. Barbero, 2013. Finite element analysis of composite materials using ANSYS (second edition), John Wiley & Sons, Ltd.

B.Crossland, 1956. Effect of large hydrostatic pressures on the torsional fatigue strength of an alloy steel, Proc. Int. Conf. Fatigue Met. Inst. Mech. Eng., pp. 138–149.

C. Navarro, S. Muñoz, and J. Domínguez, 2008. On the use of multiaxial fatigue criteria for fretting fatigue life assessment, Int. J. Fatigue, vol. 30, no. 1, pp. 32–44.

G. Sines, 1955. Failure of Materials Under Combined Repeated Stresses with Superimposed Static Stresses, NACA Tech. Note 3495, no. November, p. 72.